Journal of Hazardous Materials 321 (2017) 210–217

Contents lists available at ScienceDirect

Journal of Hazardous Materials

journal homepage: www.elsevier.com/locate/jhazmat

Innovative nanoporous carbons with ultrahigh uptakes for capture and reversible storage of CO_2 and volatile iodine

Hanxue Sun [a], Peiqing La [a], Ruixia Yang [b], Zhaoqi Zhu [a], Weidong Liang [a], Baoping Yang [a], An Li [a,*], Weiqiao Deng [b,*]

[a] College of Petrochemical Technology, Lanzhou University of Technology, Langongping Road 287, Lanzhou 730050, PR China, PR China
[b] State Key Laboratory of Molecular Reaction Dynamics, Dalian National Laboratory for Clean Energy, Dalian Institute of Chemical Physics, Chinese Academy of Sciences, Dalian 116023, PR China

HIGHLIGHTS

- Cigarette filter was utilized to prepare highly porous carbons as super absorbents.
- The porous carbons exhibit excellent iodine uptake.
- The porous carbons show high CO_2 adsorption capacity of 6.0 mmol g^{-1} at 273 K.

ARTICLE INFO

Article history:
Received 18 June 2016
Received in revised form 22 August 2016
Accepted 5 September 2016
Available online 6 September 2016

Keywords:
Iodine uptake
Porous carbon
Sustainability
Adsorption

ABSTRACT

Porous carbons as solid-state adsorbents have recently attracted considerable interest in the areas of storage and capture of CO_2 as well as the adsorption of radioactive matters. In this work, cigarette butts, one kind of common wastes referring to the filters, were utilized to prepare highly porous carbons by KOH activation in argon atmosphere. The resulting porous carbon shows a high specific surface area of up to 2751 m^2 g^{-1} with abundant micropores. The resulting porous carbon exhibits excellent iodine uptake of 262 wt% and high CO_2 adsorption capacity of 6.0 mmol g^{-1} at ambient pressure and 273 K, which both are among the highest values reported to date. Given these excellent iodine uptake, CO_2 adsorption capacity, ease of preparation as well as good physiochemical stability, the porous carbons derived from cigarette butts show great potential in the reversible adsorption of radioactive iodine and CO_2.

1. Introduction

Porous carbons have attracted considerable interest in many technologically important applications such as catalyst supports, gas storage and separation, water purification, supercapacitor *etc* [1–4], due to their numerous advantages including high surface areas, excellent electrical conductivity, good chemical and thermal stability, environmental friendliness and the possibility of tuning their textural and structural characteristics [5,6]. As promising adsorbents, they have been regarded in recent years as one of the potential materials for gas (H_2, CH_4 and CO_2 *etc.*) capture and removal of hazardous species from water [7,8]. For development of novel carbon-based porous materials with excellent adsorption performance, the challenge is how to achieve the desirable properties such as large special surface area and efficient porosities in micro-, meso- or macropores with an economic cost.

Normally, the properties of porous carbons vary with the treatment temperature, soaking time and activating agents and depend much on the type of precursors. To date, several porous carbon materials derived from various polymeric and nonpolymeric products, with structural flexibility and high surface areas (above 1000 m^2 g^{-1}) have been designed and prepared by physical or chemical activation for promising superadsorbents [9–14]. For example, Park et al. synthesized crystalline metal organic frameworks (MOFs)-derived hierarchically porous carbon with a special surface area up to 3174 m^2 g^{-1} and exceptional hydrogen storage capacity [9]. Uyama et al. prepared highly porous N-doped carbon monoliths with unprecedented CO_2 uptake by carbonization and physical activation of mesoporous polyacrylonitrile monoliths in the presence of CO_2 [11]. Excellent adsorption performances were achieved by these reported porous carbons, however, the preparation of those porous carbons has limitations in either multiple

* Corresponding authors.
E-mail addresses: lian2010@lut.cn (A. Li), dengwq@dicp.ac.cn (W. Deng).

http://dx.doi.org/10.1016/j.jhazmat.2016.09.015
0304-3894/

steps, complicated techniques or high cost, which should be a big obstacle for hindering their large-scale production. Cigarette butts referring to the organic filter were mainly composed with cellulose acetate. Approximately 500,000 tons per year of cigarette butts were disposed and caused environmental problems [15]. In this work, we used cigarette butts to prepare highly porous carbons by KOH activation in argon atmosphere. The resulting porous carbon shows a high specific surface area of up to 2751 $m^2 g^{-1}$. As solid-state adsorbents, the resulting porous carbon has volatile iodine uptake of 262 wt% and CO_2 adsorption capacity of 6.0 mmol g^{-1}, which both are among the highest values reported to date. Given these excellent adsorption capacities by combination of ease of preparation, excellent recyclability and regeneration stability, the porous carbons derived from cigarette butts show great potential in commercialization for the reversible adsorption of radioactive iodine and capture of CO_2, which should be of great importance to address environmental issues.

2. Experimental

2.1. Preparation of porous carbons

In a typical procedure [7,16], three kinds of butts from local cigarettes (Purple Lanzhou, Black Lanzhou and Hongta) were collected and washed by ethanol and distilled water several times for removal of the impurities and residues. The porous carbons were synthesized by carbonization and chemical activation of the initial butts. During the carbonization, the as-received butt (~7.5 g) was placed in a tube furnace and heated to 600 °C with a heating rate of 5 °C min^{-1} under argon and then kept for 2 h. The resultant samples were denoted as AC-1 (carbonized sample from Purple Lanzhou), AC-2 (carbonized sample from Black Lanzhou) and AC-3 (carbonized sample from Hongta), respectively. The KOH activation was performed by heating the physical mixture of the carbonized samples (1.0 g) and KOH powder (5.0 g) to 800 °C with a heating rate of 2.5 °C min^{-1} and maintained for 2 h at this temperature in a tube furnace under argon atmosphere. Finally, the resulting mixture was collected and washed with aqueous HCl (1 M) and sufficient distilled water at room temperature. The resultant samples were dried at 100 °C overnight and denoted as AK-1 (activated sample from Purple Lanzhou), AK-2 (activated sample from Black Lanzhou) and AK-3 (activated sample from Hongta), respectively.

2.2. CO_2 adsorption

The CO_2 adsorption and desorption isotherms of samples were measured using a Quantachrome Autosorb-1 volumetric adsorption analyzer at 273 K and 298 K. Prior to experiment, the sample was degassed for 6 h at 120 °C below 1×10^{-3} mbar. Then CO_2 was introduced into the system after the sample was cooled down to 273 K and 298 K. The capacity of CO_2 adsorbed in terms of volume was recorded under standard temperature and pressure. The CO_2 adsorption's kinetic data were also measured and collected using the same method as mentioned above with Quantachrome Autosorb-1 analyzer at 298 K. The pressure limit was fixed at 0.15 bar.

2.3. Adsorption of iodine

Porous carbons were exposed to nonradioactive iodine vapor in a sealed vessel at 353 K and ambient pressure. Gravimetric measurements was conducted at various time intervals to determine the iodine uptake of porous carbons. The iodine uptake was caculated as $(m_2 - m_1)/m_1 \times 100$ wt%, where m_1 and m_2 are the mass of the porous carbon before and after iodine uptake. To examine the adsorption capacity of iodine in cyclohexane, the porous carbon (10 mg) was placed into the iodine/cyclohexane solution (10 mL) and kept for certain time. Then the supernatant (~2 mL) was used for UV–vis mesurement.

2.4. Release of iodine

The sample with iodine uptake (named as I_2@AK-1, 10 mg) was placed into the dry ethanol solution (10 mL) and kept for certain time. Then the supernatant (1 mL) was diluted to 4 mL voulme by ethanol and used for UV–vis mesurement.

2.5. Characterization

X-ray diffraction (XRD) pattern analysis was performed on a Rigaku D/Max-2400 diffractometer with a Cu tube source. Raman spectra were recorded using a micro-Ramam spectroscopy (JY-HR800, Jobin Yvon) with the excitation wavelength at 532 nm. Elemental analysis was obtained using Elementar Vario EL. Scanning electron microscopy (SEM) was performed on JSM-6701F after coating the samples with Au film. Transmission electron microscopy (TEM) images were measured on a FEI (Tecnai G2 TF20) microscope operating at 200 kV. The specific surface area and pore structure were investigated with a Micrometrics ASAP 2020 system using nitrogen as the adsorbate at 77 K. X-ray photoelectron emission microscopy (XPS) analysis was performed on an ESCALAB 250Xi spectrometer (ThermoFisher Scientifi). The Fourier transform infrared (FTIR) spectra were recorded from 400 to 4000 cm^{-1} on a Nicolet FT-IR 360 spectrometer by using KBr pellets. UV/Vis spectrum was recorded on a spectrophotometer (UV-2102PC, Unico).

3. Results and discussion

3.1. Structure analysis

We synthesized porous carbons (named as AK-1, AK-2 and AK-3, see Experimental Section) by carbonization and chemical activation of three kinds of butts from local cigarettes. Raman spectra could reflect the degree of structural order (Fig. 1a). The peak positioned around 1590 cm^{-1} (G-band) is common to all sp^2 carbon systems and closely related to E2g mode of graphite. The other peak at around 1345 cm^{-1} (D-band) corresponds to the presence of disorder in carbonaceous materials [17]. Normally, the integrated intensity ratio of D-band to G-band (I_D/I_G) can reflect the relative disorder of graphitic crystallinity and is widely used to characterize the defect quantity in carbon materials [18]. Obviously, the I_D/I_G of carbon samples increased after KOH activation, suggesting the increase of disorder and the existence of more defects in these AK samples. Furthermore, the powder XRD patterns (Fig. 1b) shows that all carbon samples have well-formed and broad (002) Bragg peak from turbostratic carbon at around 24°, suggesting that no pronounced graphitization occurred. An empirical parameter R which was defined as the ratio of the height of the Bragg peak to the background [19], was adopted to measure the single layer contents in the carbon samples. The R values of AK samples decreased compared with AC samples, suggesting the breakdown of aligned structural domains in the carbon matrix after KOH activation, accordance with other work [20].

The FTIR spectrum (Fig. 2a) suggests the existence of various carbon-oxygen surface groups and structures in AK-1[21,22]. The bands at 3468 cm^{-1} and 620 cm^{-1} are associated with —OH. The peak at 2923 cm^{-1}, 2851 cm^{-1} and 1458 cm^{-1} can be ascribed to the presence of aliphatic compounds. The peak at 1458 cm^{-1} and 1121 cm^{-1} are associated with C—O. The XPS indicates that the AK-1 contains mainly carbon with a small fraction of oxygen and

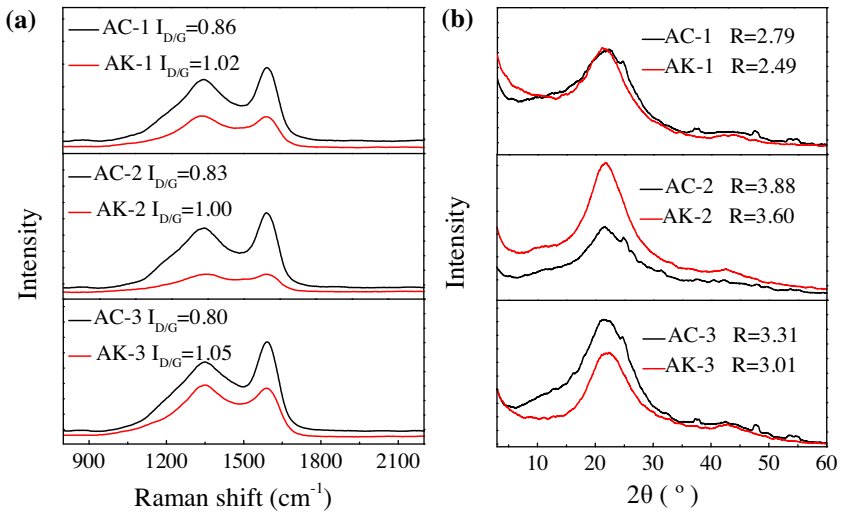

Fig. 1. (a) Raman spectra and (b) XRD patterns of porous carbons before and after KOH activation.

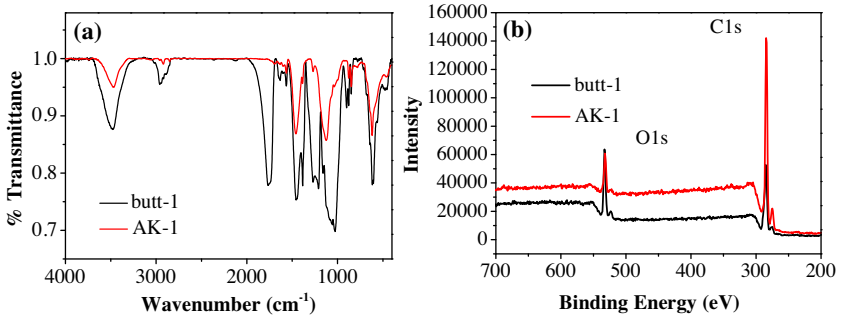

Fig. 2. (a) FTIR spectra of butt-1 and AK-1. (b) XPS spectra of butt-1 and AK-1.

further confirmed that the degree of surface oxidation for materials (Fig. 2b). The intensity of two peaks around 285.0 eV and 532.6 eV, which are contributed to C1 s and O1 s in spectra of AK-1, is enhanced greatly compared with butt-1 and the ratio of surface total oxygen to total carbon decreased from 0.44 for butt-1 to 0.07 for AK-1. Elemental analysis shows that the carbon and oxygen contents are measured to be 47.9 wt% and 47.4 wt% for butt-1, and 97.6 wt% and 1.8 wt% for AK-1 (Table S1, *Supporting information*). Results from XPS and elemental analysis suggested that the KOH activation leads to a decrease in the oxygen content and an increase in the carbon concentration (Table S1 and Fig. S1, *Supporting information*), which results in the efficient transforming from butts into micro/mesoporous carbons with unusually high specific surface areas [12].

3.2. Morphology

The raw material (taking butt-2 as an example) has a wired structure with smooth morphology (Fig. S2, *Supporting information*). After carbonization and activation, monolithic AK-2 sample shows irregular morphology with a wide range of grain size from several to tens micrometers (Fig. 3a). Higher-magnification SEM image revealed a broad range of pore widths of AK-2, from tens to hundreds nanometers (Fig. 3b). The three-dimensional network of nano-sized carbon particles with grain size of several micrometers yielded a hierarchical porous morphology of AK-2 [5]. TEM image further revealed that AK-2 exhibits a hierarchical porous texture (Fig. 3c). Also, it is clearly to see that the AK-2 is poorly crystallized and almost no parallel graphene sheets can be observed (Fig. 3d), accordance with XRD and Raman analysis. AK-1 and AK-3 have similar hierarchical porous morphology (Fig. S2 and S3, *Supporting information*). The selected area electron diffraction (SAED) pattern of the AK-2 exhibits diffusion rings patterns (Fig. S2, *Supporting information*), which further confirmed that AK-2 belongs to typical disordered carbon material.

The surface textural characteristics of carbon samples were quantified by measuring cryogenic N_2 physisorption curves. As shown in Fig. 4a, mixed type-I and –IV isotherms with well-defined plateaus were observed for all AK samples, indicating the existence of hierarchical pores with dominant microporosity in the AK samples. All carbon samples exhibit narrow BJH adsorption plots (Fig. 4b). Independent of the precursor, the pore size distribution plots indicate that the porosity of these AK samples consists of micropores with a size of ca. 2.0 nm. Here it should be noted that synthetic polymeric precursors such as polyacrylonitrile, phenolic resins and polypyrrole [23–25] have been adopted to produce porous carbon through pyrolysis method due to their low vapor pressure and high carbon yield, however, the key drawback lies in the difficulty of generating carbon materials with high special surface areas (>1000 $m^2\ g^{-1}$) as well as the formation of quality carbon coatings [26]. In this work, All AK samples achieved high special surface areas over 1600 $m^2\ g^{-1}$ (Table S2, *Supporting information*). Here it is worth emphasizing that AK-2 can achieve a high surface area of 2751 $m^2\ g^{-1}$, which is higher than that of activated carbons obtained from synthetic polymeric precursors and biomass [23–25,27]. During the activation, the carbon framework is etched by KOH to generate pores because of the oxidation of the carbon atoms, resulting in the development of micro or nano pores [7,18].

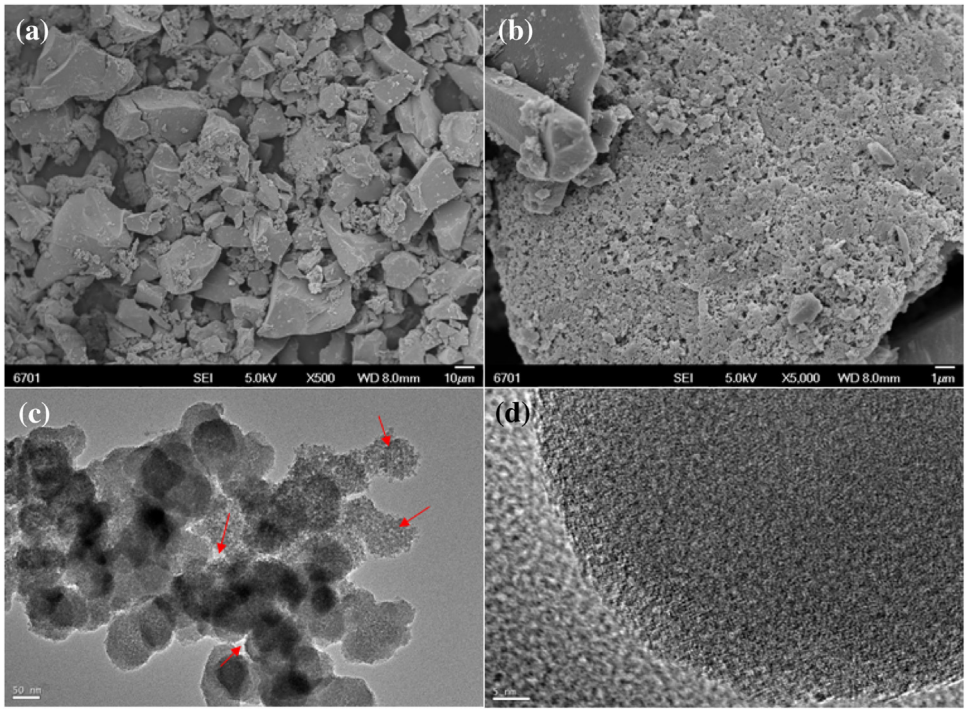

Fig. 3. (a,b) SEM images of AK-2. (c,d) TEM images of AK-2. Scale bar: (a): 10 μm, (b): 1 μm, (c): 50 nm, (d): 5 nm.

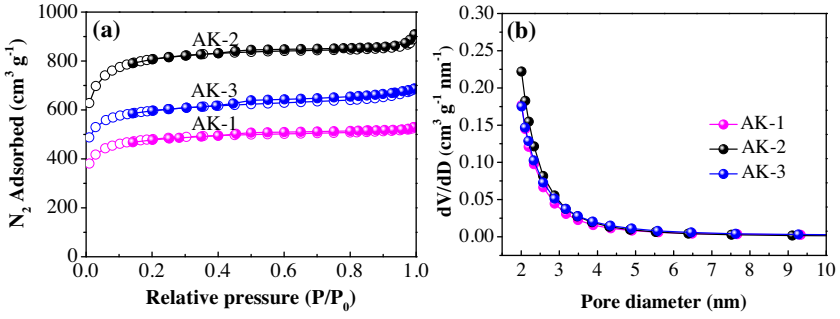

Fig. 4. (a) N_2 adsorption/desorption isotherms of activated carbons measured at 77 K. The hollow is the adsorption isotherm and solid is the desorption isotherm. (b) The pore size distribution of porous carbons.

The micropore surface areas of AK samples were between 1218 and 2033 $m^2\ g^{-1}$. The total pore volume was calculated to be 0.80, 1.34 and 1.04 $cm^3\ g^{-1}$, and the micropore volume was 0.56, 0.93 and 0.72 $cm^3\ g^{-1}$ for AK-1, AK-2 and AK-3, respectively. The percentage of micropore volume for carbon samples increased to ca. 70% after KOH activation. It should be noted that a fraction of mesopores were developed during KOH activation due to the expanding of the pre-existing micropores.

3.3. CO_2 storage

The control of anthropogenic CO_2 emissions is a great urgency in view of the significant contribution of CO_2 to global warming. To this end, porous materials such as zeolites, MOFs and microporous organic polymers have been developed for CO_2 capture and storage [28,29]. Porous carbon has also demonstrated a promising prospect in application for CO_2 capture and storage due to its high specific surface areas, low cost, availability and low energy consumption for regeneration [10,11,30]. In this case, the CO_2 adsorption capacities of the resulting porous carbons were investigated at two representative temperatures (273 K and 298 K) under low pressure by volumetric methods. As shown in Fig. 5a and b, all the porous carbons exhibit CO_2 uptake with no hysteresis between the adsorption and desorption isotherms, implying the reversible CO_2 physisorption. Table 1 summarizes the CO_2 capture capacities of the porous carbons [10,12,14,28,29,31–33]. At 273 K and low pressure (1 bar), the maximum CO_2 uptake is 5.3 mmol g^{-1} (233.2 mg g^{-1}, AK-1), 6.0 mmol g^{-1} (264.0 mg g^{-1}, AK-2) and 5.8 mmol g^{-1} (255.2 mg g^{-1}, AK-3). The amount adsorbed decreases to 3.2 mmol g^{-1} (140.8 mg g^{-1}, AK-1), 3.5 mmol g^{-1} (154.0 mg g^{-1}, AK-2) and 3.6 mmol g^{-1} (255.2 mg g^{-1}, AK-3) when the adsorption temperature increased to 298 K, which is accordance with an exothermic process such as CO_2 physisorption. Also, the CO_2 adsorption capacities of the three porous carbons are similar (5.3-6.0 mmol g^{-1} at 273 K, 3.2-3.6 mmol g^{-1} at 298 K), which is coherent with the fact that the porous characteristics of AK samples are analogous. Here it should be noted that AK-2 shows the highest CO_2 adsorption capacity of 6.0 mmol g^{-1} at 273 K due to its highest special surface area and micropore surface area. With this value, AK-2 can compete with other polymers and biomass-derived carbon materials and is still comparable to most of porous carbon materials doped with nitrogen or functionalized with amine [10,11]. More details on the comparison of the CO_2 uptakes of AK samples with other porous carbons were summarized in Table 1.

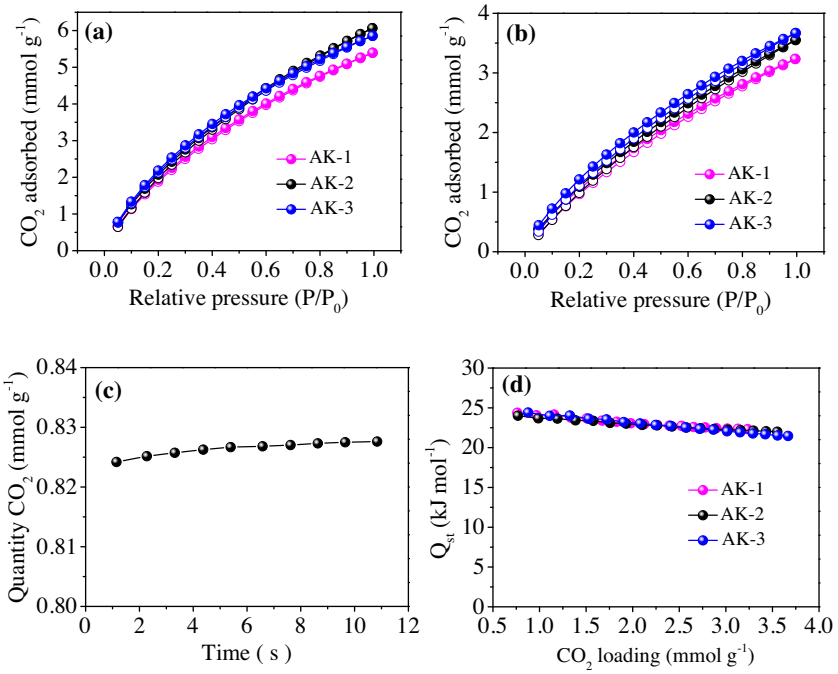

Fig. 5. CO_2 sorption isotherms of porous carbons at 273 K (a) and 298 K (b). The hollow is the adsorption isotherm and solid is the desorption isotherm. (c) Adsorption kinetic of CO_2 at 298 K for the AK-2 sample. (d) Q_{st} plots of porous carbons for the adsorption of CO_2.

Table 1
Survey of the CO_2 adsorption capacities of porous carbons in this work compared with other typical carbon materials (1 bar).

Carbon samples	S_{BET}[a] ($m^2\,g^{-1}$)	CO_2 uptakes ($mmol\,g^{-1}$)		Ref.
		273 K	298 K	
AK-1	1634	5.39	3.23	this work
AK-2	2751	6.06	3.55	this work
AK-3	2016	5.85	3.66	this work
HCM-ZC-1	808	5.4	3.8	[14]
PPN-6	4023	1.3 (295 K)		[29]
PPN-6-CH2DETA	555	4.3 (295 K)		[29]
MOP-A	4077	2.65	1.45	[28]
MOP-B	1847	3.29	1.63	[28]
MOP-C	1237	3.86	2.20	[28]
AS-4-800	2850	5.2	3.0	[30]
carbon from celtuce leaves	3404	4.36 (298 K)		[12]
carbon from polyacrylonitrile	2231	4.4 (298 K)		[31]
carbon from polypyrrole	1700	6.2	3.9	[10]
zeolite-templated carbons	3360	6.92	4.38	[32]
zeolite-templated carbons	2762	4.84	3.18	[33]

[a] S_{BET} presents the BET surface areas.

The flue gas from coal-fired power plants is approximately 15% CO_2 at total pressures of around 1 bar. Thus, the adsorption kinetics data of CO_2 on AK-2 was collected at a pressure of 0.15 bar and 298 K (Fig. 5c). The results show that AK-2 took a very short time (<5 s) to reach the adsorption equilibrium, suggesting that CO_2 diffuses very fast inside AK-2 [30].

To better understand the adsorption properties of AK-2, the isosteric heat of adsorption (Q_{st}) was calculated from the CO_2 adsorption isotherms obtained at 273 K and 298 K. The plot of the adsorption enthalpies as a function of CO_2 loading was shown in Fig. 5d. It was found that AK-2 had a heat of adsorption of more than 23.0 kJ mol^{-1} at low coverage. The Q_{st} for AK-2 decreased a little from 24.0 kJ mol^{-1} to 22.0 kJ mol^{-1} with the increase of CO_2 loading, which is different from other systems in which the Q_{st} value decreased sharply with the increase of CO_2 uptake [28,29]. Similar observations were obtained for AK-1 and AK-3. The low Q_{st} values (<25 kJ mol^{-1}) of CO_2 adsorption on the AK samples characterize weak interactions with CO_2, thus suggesting a relatively easy regeneration and fast adsorption/desorption rates [14].

3.4. Capture and reversible storage of iodine

Radioactive iodine (^{129}I, ^{131}I) produced from nuclear fission of fissile nuclides presents unique exposure problems and directly affects human metabolic processes. In particular, the nuclear accident at Fukushima, Japan in 2011 has raised awareness and underscored the urgent need for radiation protection and appropriate nuclear waste management. Thus, the capture of radioactive iodine using porous materials should be of great importance [16,34,35]. To investigate their adsorption properties for iodine, the porous carbons were exposed to nonradioactive iodine vapor in a sealed vessel at 353 K and ambient pressure. As shown in Fig. 6a, with prolonging the contact time, the mass of all porous carbons increased significantly in 3 h and no more changes in the iodine-loading amounts were observed after 12 h, indicating that

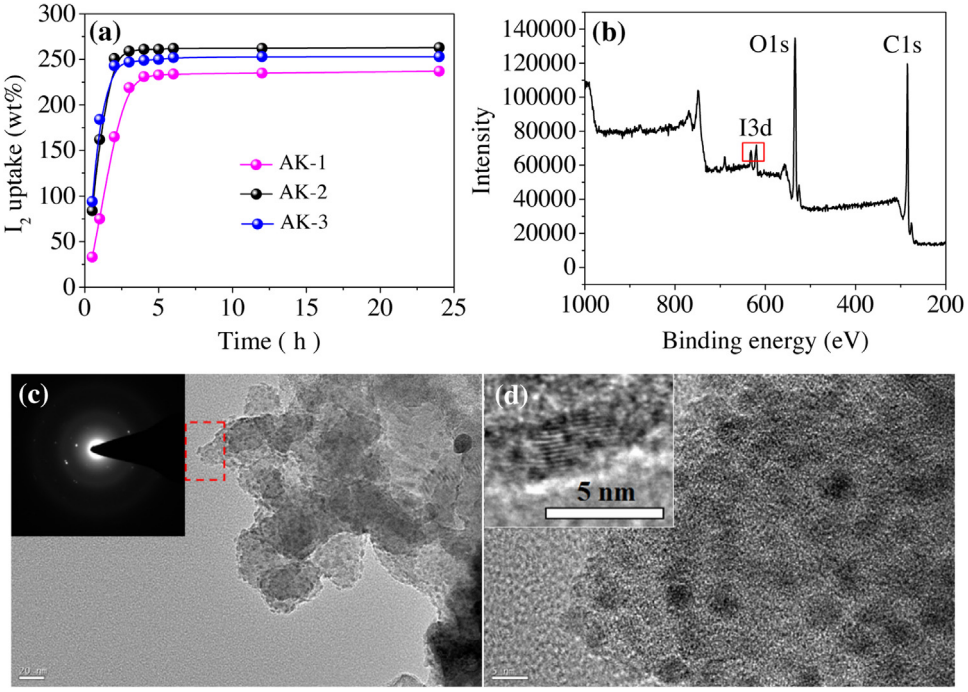

Fig. 6. (a) Gravimetric uptake of iodine as a function of time at 353 K. (b) XPS spectrum of I_2@AK-1. (c) TEM image of I_2@AK-1. Inset is the SAED pattern of I_2@AK-1. (d) HRTEM image of I_2@AK-1 in the red circle of (c), inset shows the crystal lattice of I_2 embedded in AK-1. Scale bar: (a): 20 nm, (b): 5 nm (For interpretation of the references to colour in this figure legend, the reader is referred to the web version of this article.)

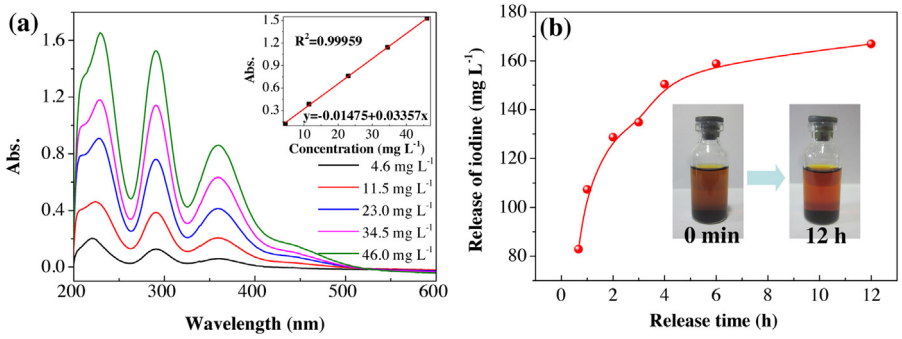

Fig. 7. (a) Calibration plot of standard iodine by UV/vis spectra in ethanol solution. Inset is the fitting of Abs value *vs* concentration of iodine in ethanol solution with the relatively good linearity satisfies Lambert-Beer Law. (b) The delivery curves of iodine from I_2@AK-1. Inset shows the iodine releasing process of I_2@AK-1 (10 mg) soaked in 10 mL of dry ethanol.

the system was basically saturated. The maximum iodine uptake is 237, 262 and 253 wt% for AK-1, AK-2 and AK-3, respectively, much higher than that of other solid adsorbents, for example, silver-based zeolites, MOFs and covalently linked porous organic polymers [28,36–40]. To our knowledge, the iodine uptake for AK-2 is the highest value for the solid adsorbents reported to date [36–43].

The iodine-loaded sample (I_2@AK-1) was characterized by XPS and TEM. XPS analysis of I_2@AK-1 confirmed the existence of iodine on AK-1 with the valence of zero, which suggested that the adsorbed iodine species exists as I_2 (Fig. 6b). TEM image shows that the I_2 crystals embedded within the AK-1 with a diameter of ~4 nm (Fig. 6d). The crystal lattice of iodine molecule could be clearly identified (inset of Fig. 6d). And the iodine crystals and corresponding lattice parameter were further observed in selected area diffraction pattern of the I_2@AK-1 (inset of Fig. 6c). These observations further suggest that the porous carbons utilized their high porosity to remove iodine molecule in gaseous state. Besides, this iodine sorption of porous carbon is reversible. The recovery of porous carbons could be performed by dissolving and completely releasing the trapped molecular iodine in organic solvents [44], such as ethanol. When I_2@AK-1 was soaked in dry ethanol, the color of the ethanol solution turned dark brown, indicating that the iodine molecules were dissociated from the solid. Fig. 7 shows that the delivery of iodine in ethanol increases nonlinearly with time increasing, suggesting that the iodine release is mainly governed by a free diffusion process [45].

In addition, the trapping iodine can be conducted in solution using the sythesized porous carbons. Taking the AK-2 as an example, the AK-2 exhibited a similar adsorption behaviour in iodine/cyclohexane solutions with different concentration (Fig. 8a). That is, the adsorption capacity initially increased quickly with increasing of contact time and then gradually reached equilibrium after 24 h. Meanwhile, the color of the iodine/cyclohexane solution turned paler with an increase of contact time. The adsorption capacity with an iodine uptake reaches up to 336 mg g^{-1} for

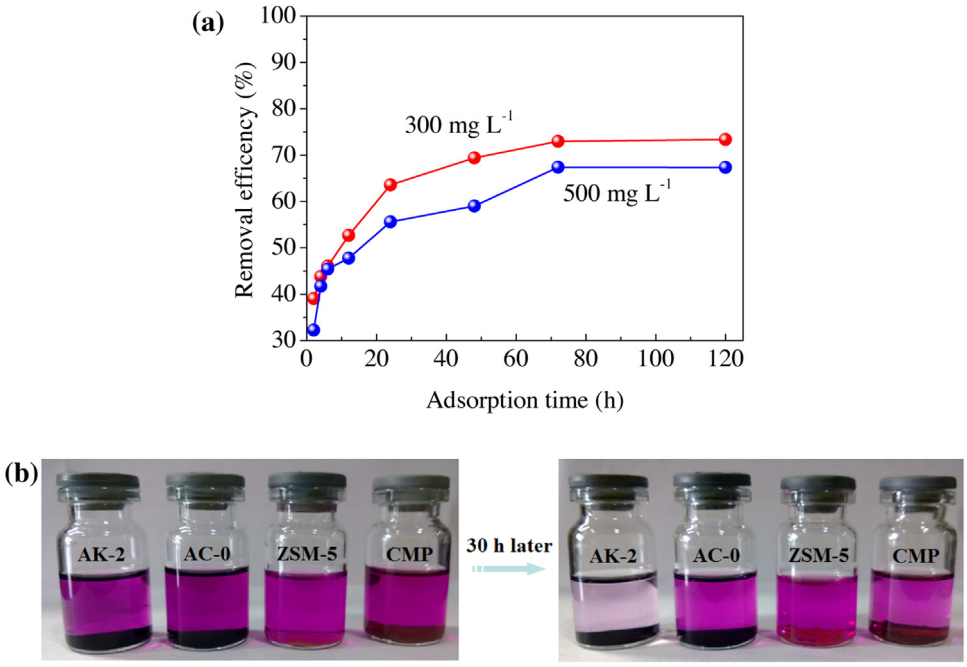

Fig. 8. (a) The removal efficency of iodine by AK-2 in cyclohexane solutions with different concertation of 300 mg L^{-1} and 500 mg L^{-1}. (b) The photographs display the adsorption degrees of AK-2, commerical activated carbon (AC-0), ZSM-5 and CMP.

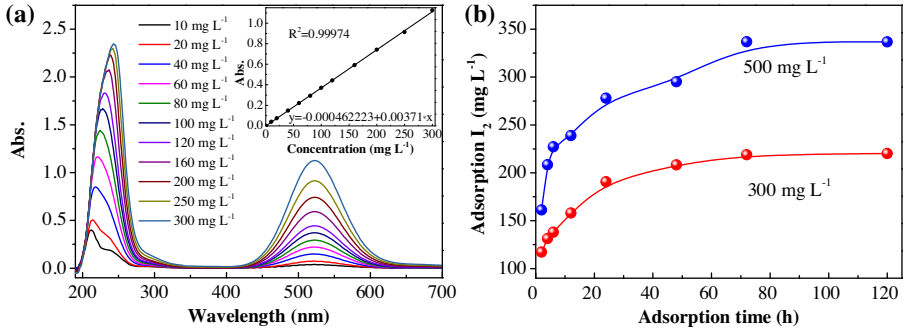

Fig. 9. (a) Calibration plot of standard iodine by UV/vis spectra in cyclohexane solution. Inset is the fitting of Abs value *vs* concentration of iodine in cyclohexane solution with the relatively good linearity satisfies Lambert-Beer Law. (b) The kinetic studies of iodine adsorption by AK-2 in cyclohexane solutions with different concentration of 300 mg L^{-1} and 500 mg L^{-1}.

AK-2 in iodine solution of 500 mg L^{-1} (Fig. 9), higher than that of metalloporphyrin-based CMP [39], which should be contributed the excellent porosity. Removal efficiencies of 73% and 67% for AK-2 in 300 mg L^{-1} and 500 mg L^{-1} of iodine/cyclohexane solution were obtained (Fig. 8a). Fig. 8b displays the same weights (10 mg) of different adsorbents in a 10 mL iodine/cyclohexane solution with a same concentration of 300 mg L^{-1}. Results show that the adsorption of iodine on AK-2 is remarkable and clearly exceeds that of zeolite (ZSM-5) and CMP in the iodine/cyclohexane solution.

4. Conclusions

In conclusion, we have synthesized novel porous carbons derived from cigarette butts by KOH activation. The resulting porous carbons show high specific surface areas between 1634 m^2 g^{-1} and 2751 m^2 g^{-1} with high micropores ratio. As adsorbents, the resulting carbon samples exhibit high CO_2 adsorption capacity with a maximum value of 6.0 mmol g^{-1} at 273 K. Besides, the resulting carbon samples show exceptionally high capacity of 262 wt% for iodine vapor capture. Taking advantages of the excellent CO_2 capture capacity, high iodine uptake, ease of preparation, physicochemical stability as well as low cost, the porous carbons derived from cigarette butts should hold immense promise in post-combustion capture of CO_2 and reversible adsorption radioactive matters applications.

Acknowledgements

The authors are grateful to the National Natural Science Foundation of China (Grant No. 51263012, 51262019, 51462021, 51663012 and 51403092), Support Program for Hongliu Young Teachers (Q201411), Hongliu Elitist Scholars of LUT (J201401) and Fundamental Research Funds for the Universities of Gansu Province, the National Natural Science Fund for distinguished young scholars (Grant No. 21525315).

Appendix A. Supplementary data

Supplementary data associated with this article can be found, in the online version, at http://dx.doi.org/10.1016/j.jhazmat.2016.09.015.

References

[1] N. Hiyoshi, O. Sato, A. Yamaguchi, C.V. Rode, M. Shirai, Kinetic analysis of 4-isopropylphenol hydrogenation over activated carbon-supported rhodium catalysts in supercritical carbon dioxide solvent, Green Chem. 14 (2012) 633–638.
[2] M. Choi, R. Ryoo, Mesoporous carbons with KOH activated framework and their hydrogen adsorption, J. Mater. Chem. 17 (2007) 4204–4209.
[3] H. Sun, A. Li, Z. Zhu, W. Liang, X. Zhao, P. La, W. Deng, Superhydrophobic activated carbon-coated sponges for separation and absorption, ChemSusChem 6 (2013) 1057–1062.
[4] J.W. Beidaghi, M. Hatzell, K.B. Dennison, C.R. Musci, B.V. Presser, E.C. Kumbur, Y. Gogotsi, Investigation of carbon materials for use as a flowable electrode in electrochemical flow capacitors, Electrochim. Acta 98 (2013) 123–130.
[5] S. Dutta, A. Bhaumik, K.C.-W. Wu, Hierarchically porous carbon derived from polymers and biomass: effect of interconnected pores on energy applications, Energy Environ. Sci. 7 (2014) 3574–3592.
[6] Y. Xia, Z. Yang, R. Mokaya, Templated nanoscale porous carbons, Nanoscale 2 (2010) 639–659.
[7] H. Wang, Q. Gao, J. Hu, High hydrogen storage capacity of porous carbons prepared by using activated carbon, J. Am. Chem. Soc. 131 (2009) 7016–7022.
[8] H. Qin, P. Gao, F. Wang, L. Zhao, J. Zhu, A. Wang, T. Zhang, R. Wu, H. Zou, Highly efficient extraction of serum peptides by ordered mesoporous carbon, Angew. Chem. Int. Ed. 50 (2011) 12218–12221.
[9] S.J. Yang, T. Kim, J.H. Im, Y.S. Kim, K. Lee, H. Jung, C.R. Park, MOF-derived hierarchically porous carbon with exceptional porosity and hydrogen storage capacity, Chem. Mater. 24 (2012) 464–470.
[10] M. Sevilla, P. Valle-Vigón, A.B. Fuertes, N-doped polypyrrole based porous carbons for CO_2 capture, Adv. Funct. Mater. 21 (2011) 2781–2787.
[11] M. Nandi, K. Okada, A. Dutta, A. Bhaumik, J. Maruyama, D. Derks, H. Uyama, Unprecedented CO_2 uptake over highly porous N-doped activated carbon monoliths prepared by physical activation, Chem. Commun. 48 (2012) 10283–10285.
[12] R. Wang, P. Wang, X. Yan, J. Lang, C. Peng, Q. Xue, Promising porous carbon derived from celtuce leaves with outstanding supercapacitance and CO_2 capture performance, ACS Appl. Mater. Interfaces 4 (2012) 5800–5806.
[13] Y.-S. Bae, R.Q. Snurr, Development and evaluation of porous materials for carbon dioxide separation and capture, Angew. Chem. Int. Ed. 50 (2011) 11586–11596.
[14] D. Qian, C. Lei, E. Wang, W. Li, A. Lu, A method for creating microporous carbon materials with excellent CO_2-adsorption capacity and selectivity, ChemSusChem 7 (2014) 291–298.
[15] S.M. Soltani, S.K. Yazdi, S. Hosseini, Effects of pyrolysis conditions on the porous structure construction of mesoporous charred carbon from used cigarette filters, Appl. Nanosci. 4 (2014) 551–569.
[16] H. Sun, P. La, Z. Zhu, W. Liang, B. Yang, An Li, Capture and reversible storage of volatile iodine by porous carbon with high capacity, J. Mater. Sci. 50 (2015) 7326–7332.
[17] A. Cuesta, P. Dhamelincourt, J. Laureyns, A. Martinez-Alonso, J.M.D. Tascon, Raman microporobe studies on carbon materials, Carbon 32 (1994) 1523–1532.
[18] L. Qie, W. Chen, H. Xu, X. Xiong, Y. Jiang, F. Zou, X. Hu, Y. Xin, Z. Zhang, Y. Huang, Synthesis of functionalized 3D hierarchical porous carbon for high-performance supercapacitors, Energy Environ. Sci. 6 (2013) 2497–2504.
[19] Y. Liu, J.S. Xue, T. Zheng, J.R. Dahn, Mechanism of lithium insertion in hard carbons prepared by phrolysis of epoxy resins, Carbon 34 (1996) 193–200.
[20] D. Lozano-Castelló, J.M. Calo, D. Cazorla-Amorós, A. Linares-Solano, Carbon activation with KOH as explored by temperature programmed techniques and the effects of hydrogen, Carbon 45 (2007) 2529–2536.
[21] S.M. Soltani, S.K. Yazdi, S. Hosseini, I. Bayestie, Lead removal from aqueous solution using non-modified and nitric acid-modified charred carbon from the pyrolysis of used cigarette filters, Desalin. Water Treat. 53 (2014) 126–138.
[22] S.M. Soltani, S.K. Yazdi, S. Hosseini, M.K. Gargari, Effect of nitric acid modification on porous characteristics of mesoporous char synthesized from the pyrolysis of used cigarette filters, J. Environ. Chem. Eng. 2 (2014) 1301–1308.
[23] C.M. Yang, C. Weidenthaler, B. Spliethoff, M. Mayanna, F. Schuth, Facile template synthesis of ordered mesoporous carbon with polypyrrole as carbon precursor, Chem. Mater. 17 (2005) 355–358.
[24] A. Lu, A. Kiefer, W. Schmidt, F. Schuth, Synthesis of polyacrylonitrile-based ordered mesoporous carbon with tunable pore structures, Chem. Mater. 16 (2004) 100–103.
[25] J. Hayashi, M. Uchibayashi, T. Horikawa, K. Muroyama, V.G. Gomes, Synthesizing activated carbons from resins by chemical activation with K_2CO_3, Carbon 40 (2002) 2747–2752.
[26] J.S. Lee, X. Wang, H. Luo, G.A. Baker, S. Dai, Facile ionothermal synthesis of microporous and mesoporous carbons from task specific ionic liquids, J. Am. Chem. Soc. 131 (2009) 4596–4597.
[27] L. Wei, M. Sevilla, A.B. Fuertes, R. Mokaya, G. Yushin, Hydrothermal carbonization of abundant renewable natural organic chemicals for high-performance supercapacitor electrodes, Adv. Energy Mater. 1 (2011) 356–361.
[28] R. Dawson, E. St€ockel, J.R. Holst, D.J. Adams, A.I. Cooper, Microporous organic polymers for carbon dioxide capture, Energy Environ. Sci. 4 (2011) 4239–4245.
[29] W. Lu, J.P. Sculley, D. Yuan, R. Krishna, Z. Wei, H. Zhou, Polyamine-tethered porous polymer networks for carbon dioxide capture from flue gas, Angew. Chem. Int. Ed. 51 (2012) 7480–7484.
[30] M. Sevilla, A.B. Fuertes, Sustainable porous carbons with a superior performance for CO_2 capture, Energy Environ. Sci. 4 (2011) 1765–1771.
[31] W. Shen, S. Zhang, Y. He, J. Li, W. Fan, Hierarchical porous polyacrylonitrile-based activated carbon fibers for CO_2 capture, J. Mater. Chem. 21 (2011) 14036–14040.
[32] Y. Xia, R. Mokaya, G.S. Walker, Y. Zhu, Superior CO_2 adsorption capacity on N-doped high-surface-area, microporous carbons templated from zeolite, Adv. Energy Mater. 1 (2011) 678–683.
[33] D.F. Sava, M.A. Rodriguez, K.W. Chapman, P.J. Chupas, J.A. Greathouse, P.S. Crozier, T.M. Nenoff, Capture of Volatile Iodine A gaseous fission product, by zeolitic imidazolate framework-8, J. Am. Chem. Soc. 133 (2011) 12398–12401.
[34] X. Qian, Z. Zhu, H. Sun, F. Ren, P. Mu, W. Liang, L. Chen, A. Li, Capture and reversible storage of volatile iodine by novel conjugated microporous polymers containing thiophene units, ACS Appl. Mater. Interface 8 (2016) 21063–21069.
[35] F. Ren, Z. Zhu, X. Qian, W. Liang, P. Mu, H. Sun, J. Liu, A. Li, Novel thiophene-bearing conjugated microporous polymer honeycomb-like porous spheres with ultrahigh iodine uptake, Chem. Commun. 52 (2016) 9797–9800.
[36] K.W. Chapman, P.J. Chupas, T.M. Nenoff, Radioactive iodine capture in silver-containing mordenites through nanoscale silver iodide formation, J. Am. Chem. Soc. 132 (2010) 8897–8899.
[37] Q. Liu, J. Ma, Y. Dong, Highly efficient iodine species enriching and guest-driven tunable luminescent properties based on a cadmium(II)-triazole MOF, Chem. Commun. 47 (2011) 7185–7187.
[38] P.-S. Huang, C.-H. Kuo, C.-C. Hsieh, Y.-C. Horng, Selective capture of volatile iodine using amorphous molecular organic solids, Chem. Commun. 48 (2012) 3227–3229.
[39] A. Sigen, Y. Zhang, Z. Li, H. Xia, M. Xue, X. Liu, Y. Mu, Highly efficient and reversible iodine capture using a metalloporphyrin-based conjugated microporous polymer, Chem. Commun. 50 (2014) 8495–8498.
[40] D.F. Sava, K.W. Chapman, M.A. Rodriguez, J.A. Greathouse, P.S. Crozier, H. Zhao, P.J. Chupas, T.M. Nenoff, Competitive I_2 sorption by Cu-BTC from humid gas streams, Chem. Mater. 25 (2013) 2591–2596.
[41] T. Hasell, M. Schmidtmann, A.I. Cooper, Molecular doping of porous organic cages, J. Am. Chem. Soc. 133 (2011) 14920–14923.
[42] C.-C. Chien, Y.-P. Huang, W.-C. Wang, J.-H. Chao, Y.-Y. Wei, Efficiency of Moso Bamboo charcoal and activated carbon for adsorbing radioactive iodine, Clean-Soil Air Water 39 (2011) 103–108.
[43] J. Zhou, S. Hao, L. Gao, Y. Zhang, Study on adsorption performance of coal based activated carbon to radioactive iodine and stable iodine, Ann. Nucl. Energy 72 (2014) 237–241.
[44] Y. Chen, H. Sun, R. Yang, T. Wang, C. Pei, Z. Xiang, Z. Zhu, W. Liang, A. Li, W. Deng, Synthesis of conjugated microporous polymer nanotubes with large surface areas as absorbents for iodine and CO_2 uptake, J. Mater. Chem. A 3 (2015) 87–91.
[45] M. Zeng, Q. Wang, Y. Tan, S. Hu, H. Zhao, L. Long, M. Kurmoo, Rigid pillars and double walls in a porous metal-organic framework: single-crystal to single-crystal, controlled uptake and release of iodine and electrical conductivity, J. Am. Chem. Soc. 132 (2010) 2561–2563.